The Aeronautical Journal (2025), **129**, pp. 3227–3251
doi:10.1017/aer.2025.10042

ROYAL AERONAUTICAL SOCIETY

RESEARCH ARTICLE

A singular perturbation-based adaptive control strategy for flexible joint space manipulators with joint friction

B. Qiao, S. Huang and Z. Huang

College of Astronautics, Nanjing University of Aeronautics and Astronautics, Nanjing, China
Corresponding author: B. Qiao; Email: bqiao@nuaa.edu.cn

Received: 26 July 2024; **Revised:** 25 May 2025; **Accepted:** 28 May 2025

Keywords: flexible joint; adaptive controller; singular perturbation; friction compensation

Abstract

Harmonic drives, commonly utilised in space manipulators for high transmission ratios and efficient energy transfer, introduce joint flexibility that leads to issues such as hysteresis, vibration and nonlinear coupling. An adaptive control approach with friction compensation is proposed for flexible joint space manipulators to mitigate joint flexibility and address nonlinear friction issues. According to singular perturbation decoupling, the dynamic system of space manipulators is decomposed into two second-order subsystems with distinct time scales. By introducing the concept of an integral manifold, the two subsystems of fast and slow are refactored into two distinct tracking systems. For the slow subsystem, an adaptive control scheme with friction compensator is designed, employing an enhanced linear parameterisation expression. The friction compensator is designed with a decomposition-based compensation control scheme. Meanwhile, a proportional-derivative (PD) controller is provided for the refactored fast subsystem, which avoids incorporating second-order derivative terms of elastic torques into the proposed controller, thereby enhancing computational efficiency and engineering practicability. Approximate differential filters are utilised to estimate the joint velocities of the links and the differential terms of joint elastic torques, which reduces noise disturbances and improves the robustness of the control system. Notably, a modified compensation scheme is proposed to solve the problem that the conventional singular perturbation method is limited to be utilised in space manipulators with weak joint flexibility. Furthermore, the stability proof of the entire system is conducted according to the Lyapunov stability theorem. Ultimately, simulations and analyses demonstrate that the provided strategy is effective.

Nomenclature

$H_l(q)$	the links' inertia matrix
$C(q,\dot{q})$	the matrix related to Coriolis and centrifugal efforts
$q,\dot{q},\ddot{q}$	generalised position, velocity and acceleration vector of links
$\theta,\dot{\theta},\ddot{\theta}$	generalised position, velocity and acceleration vector of actuators
H_m	the actuator inertia matrix
$\tau \in R^n$	the elastic torques vector between motors and manipulator's links
$\tau_{fr} \in R^n$	non-linear friction torque
$\tau_m \in R^n$	the control input torques vector of the actuator
B_i	the viscous friction coefficient
F_{ci}	the Coulomb friction-related parameter
F_{si}	the static friction-related parameter
$F_{\tau i}$	a positive parameter corresponding to the Stribeck effect
F_{ui}	the position dependency of friction and various friction modeling errors
$\hat{B}_i, \hat{F}_{ci}, \hat{F}_{si}$ and $\hat{F}_{\tau i}$	the nominal values of B_i, F_{ci}, F_{si} and $F_{\tau i}$
$P \in R^r$	the vector of manipulator parameters
$Y(q,\dot{q},\ddot{q})$	a known regressor matrix

© The Author(s), 2025. Published by Cambridge University Press on behalf of Royal Aeronautical Society.

https://doi.org/10.1017/aer.2025.10042 Published online by Cambridge University Press

K	the stiffness coefficient
h	a sufficiently smooth function
μ	the small enough perturbation coefficient
τ_s	the control input torque of the slow subsystem
τ_f	the control input torque of the fast subsystem
τ_f^*	the control input torque of the refactored fast subsystem
$\bar{\tau}_s$	the corrective slow subsystem control input torque
$\bar{\tau}_f$	the corrective fast subsystem control input torque
τ_1	the corrective control term
s	sliding surface
e	trajectory tracking error
$\dot{e}$	velocity tracking error
$q_d(t)$	desired trajectory
h_i, ε_{pvn}^i, ε^i, ρ_{fi}	unknown constants
λ_c, K_s, Λ, w_{1i}, w_{2i}	positive constants
$v \in R^n$	the approximate differential signal
φ	an introduced auxiliary variable

1.0 Introduction

As humanity's exploration of space continues, space manipulators play pivotal roles in space exploration, adept at various on-orbit services like capturing satellites and space debris, [1, 2] Fig. 1. Representative examples include Canadarm2, a key component of the International Space Station (ISS), which has demonstrated exceptional capabilities in module installation, payload handling, and assisting astronauts during extravehicular activities. With its seven-joint design and end-over-end walking capability, it can traverse the ISS structure to perform complex operations [34]. Similarly, Redwire's STAARK is a next-generation modular autonomous robotic arm developed for the maintenance and assembly of small spacecraft. It supports modern on-orbit missions including rendezvous, docking and modular payload handling in both geostationary orbit (GEO) and low-earth orbit (LEO), and is also being prototyped for use with the Argonaut lunar lander, extending its application to future lunar missions [35]. These manipulators not only enhance mission efficiency but also significantly reduce the risk associated with astronauts leaving the capsule. The European Robotic Orbital Support Services (EROSS) represents a landmark initiative in space manipulators, designed to demonstrate next-generation technologies for critical on-orbit servicing operations encompassing propellant replenishment, modular component replacement, and in-situ maintenance. By integrating high-precision robotic arms, sophisticated guidance and navigation systems, and autonomous control algorithms, EROSS enables the safe capture and manipulation of client satellites. This significantly enhances the operational capabilities of robotic systems in space while improving the autonomy and reliability of future orbital servicing missions [36]. Generally, lightweight and long-reaching manipulators are favoured to minimise launch mass and expand operational workspace. Nevertheless, a significant issue with such lightweight space manipulators is the increased link flexibilities, which result in structural vibrations, particularly when handling heavy payloads. Additionally, joint flexibilities, which are mostly brought on by harmonic drives, could impact space manipulators [3].

This paper focuses on considering joint flexibilities solely. For space manipulators, like the free-floating/flying space manipulator systems under investigation, or for flight systems in previous and ongoing on-orbit services missions such as deutscher orbital service system (DEOS) [4] and e. Deorbit [5], the assumption is reasonable. Such flexibilities can lead to substandard performance when handling heavy payloads, potentially causing elastic deformation and system vibration. These issues have a negative impact on the trajectory tracking precision and quicken the wear and tear of flexible components. Additionally, the strong coupling between joint friction and joint flexibility becomes more pronounced, amplifying the nonlinear features of joint friction when space manipulators move at low speed. This

https://doi.org/10.1017/aer.2025.10042 Published online by Cambridge University Press

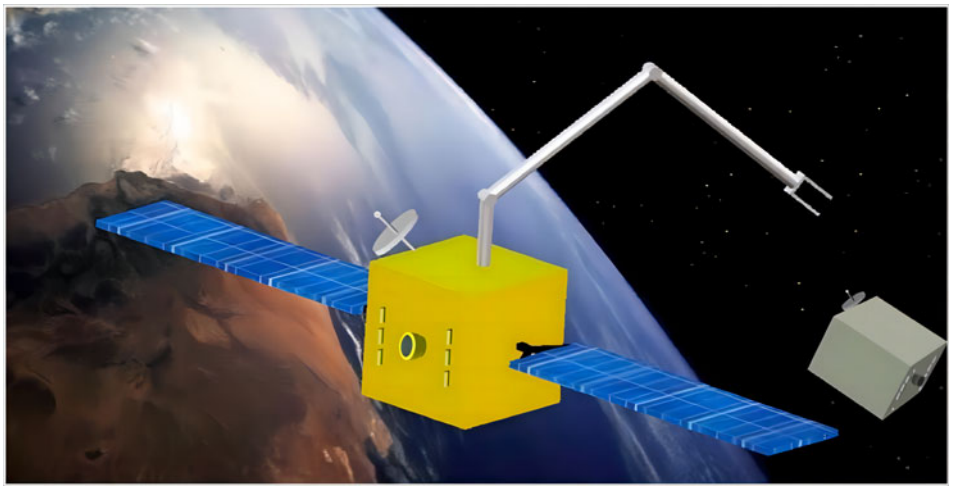


Figure 1. *A space manipulator operating on-orbit.*

exacerbates control challenges, rendering the space manipulators less effective in their operations. To achieve highly accurate trajectory tracking, it is crucial to concurrently consider the impacts of joint flexibility and joint friction.

The dynamics modeling and control problems have been the main topics of previous research on space manipulators with flexible joints. In practical engineering applications, obtaining an accurate mathematical model of a space manipulator poses significant challenges. It is necessary to introduce reasonable approximations during the modeling process to account for uncertainties in certain system parameters. Considering these parameter uncertainties, advanced adaptive control strategies can be employed. Adaptive control techniques mitigate the effects of model parameter uncertainties on control performance by dynamically adjusting parameters in real-time. This approach ensures system asymptotic stabilisation or that steady-state tracking errors tend towards zero, without requiring high gain conditions. Several adaptive control strategies, as detailed in references [6, 7], have been proposed, specifically addressing the issue of parametric uncertainties through adaptive techniques. A fully dynamic feedforward compensation component and a PD feedback component comprise the computationally straightforward and efficient adaptive tracking controllers that Slotine and Li presented [8]. Online parameter estimation is used to determine the payload and unknown manipulator. To mitigate the elastic oscillation at the joints, Spong introduced a straightforward correction term to the controller for manipulators and provided a new singular perturbation-based adaptive controller for a flexible-joint manipulator [9, 10]. The adaptive compensation control method that Huang et al. described enables precise trajectory tracking and the limited torque errors for a flexible joint manipulator with limited mobility and uncertain parameters [11]. The controller uses joint state variables feedback, avoiding the commonly found noisy joint torque measurements in other controllers. Moreover, some researchers combined fuzzy and neural network with adaptive control law to propose compensatory control approaches for flexible-joint manipulators. To address the model uncertainties, Subudhi and Morris proposed a strategy in which the radial basis function neural network was used for the slow control and a linear-quadratic fast control [12]. As research continues to progress, extended adaptive control schemes are provided. The provided adaptive controller compensates for the friction brought on by harmonic drives, while considering the dynamic characteristics of the joint flexibility. However, methods take only static friction into account [13, 14]. The space manipulator's dynamic model considering joint friction was provided by Zhang et al., employing the single direction recursive construction method and Jourdain's velocity variation concept. By utilising the computed torque approach, a trajectory tracking control strategy that includes friction compensation is proposed [15].

https://doi.org/10.1017/aer.2025.10042 Published online by Cambridge University Press

Recently, innovative control strategies have been developed to address the challenges posed by hybrid uncertainties in vibration active control systems. For instance, Li et al. proposed a proportional–integral–derivative (PID) controller design based on probability density evolution method and interval-oriented sequential optimisation strategy [37], which effectively handles both interval and random uncertainties. This approach not only enhances the reliability of the control system but also balances energy consumption and safety. Similarly, Wang et al. introduced a Kriging-based decoupled non-probability reliability-based design optimisation scheme for piezoelectric PID control systems [38]. This method decouples uncertainty parameters and design variables, significantly improving computational efficiency while maintaining accuracy. These advancements highlight the ongoing efforts to enhance control strategies for systems with complex uncertainties.

Joint friction is initially described utilising the Coulomb friction model. Subsequently, various models have been developed, including the LuGre model, which effectively captures most friction behaviour [16]. The literature has taken the combined influence of joint flexibility and friction into consideration. Research has concentrated on identifying and compensating for joint friction in a manipulator. The friction compensation algorithm is composed of a single-state dynamic model that describes the friction torque [17]. An adaptive control strategy was provided by M. Feemster to compensate for linear parametric friction in a second-order mechanical system that includes frictional effects such as Coulomb, static, Stribeck and viscous friction. The Stribeck parameter is assumed to be accurately known [18]. For the complicated friction features, H. Gao constructed a precise and effective hybrid friction model incorporating static, Coulomb and Stribeck friction, where velocity acts as the determining factor for switching between friction types [19]. Although the previous control laws can effectively achieve accurate tracking of positions and mitigate structural vibration for flexible joint space manipulators, there are currently few control strategies designed to compensate joint friction for flexible joint space manipulators. It is challenging to carry out position tracking control and vibration suppression rapidly and accurately because joint flexibility can cause oscillation, and joint friction may reduce tracking efficiency.

The primary contributions of this paper are that an adaptive control strategy based on singularly perturbed decoupling is provided for flexible-joint space manipulators to mitigate joint flexibility and address nonlinear joint friction issues when parametric uncertainties and joints friction are present. This control strategy consists of the following three primary parts:

1. A novel decomposition-based friction compensation scheme is designed to compensate for joint friction.
2. A modified compensation scheme is proposed to solve the problem that the conventional singular perturbation method is limited to be utilised in space manipulators with weak joint flexibility.
3. A composite adaptive control scheme according to singular perturbation decoupling is proposed to compensate for joint flexibility.

A nonlinear experimental friction model is linearised in parameters to provide a linear parametric friction model, which describes joint friction. The friction compensator is designed with the compensation control scheme based on decomposition. The essential principle of the decomposition-based modeling and control strategy lies in distinguishing between different types of uncertain parameters and variables, designing separate compensators for each, and considering each physical characteristic. The strategy aims to deal with various kinds of model uncertainty in appropriate way, which makes it possible to target different types of friction characteristics more precisely. The performance of mechanical systems under friction model uncertainty can be significantly enhanced by employing a combination of adaptive and robust compensators.

The singular perturbation technique is a highly effective method for managing complex systems with multi-scale features. Since M.W. Spong first demonstrated its feasibility for modeling and control, it has been widely applied in the study of flexible joint space manipulators. This approach offers the advantage of model reduction, decomposing the original high-order system into two low-order subsystems.

https://doi.org/10.1017/aer.2025.10042 Published online by Cambridge University Press

This decomposition facilitates the design of corresponding controllers, simplifies the overall control strategy design process, and allows for detailed dynamic analysis of each subsystem. However, the conventional singular perturbation method is typically suitable solely for manipulators with weak joint flexibility. A modified compensation scheme is proposed to enhance system stiffness and address deviations, thereby overcoming the limitations imposed on traditional singular perturbation methods. This enhancement is achieved by incorporating a compensation term into the control law. According to the concept of integral manifolds, this compensation term is designed to improve system stiffness, enabling the control system to manage joint flexibility more effectively.

To compensate for joint flexibility, a composite controller is designed for flexible joint space manipulators. The inertias of the rotors, including gear reduction, which have often been neglected in previous research, are taken into account in the process of modeling the dynamics in this paper in order to build a more accurate dynamics model. By introducing the concept of integral manifolds, the two subsystems, fast and slow, obtained based on singular perturbation decoupling are refactored into two different tracking systems, which facilitates the development of the system control approach. First, for the slow subsystem, an adaptive control scheme with friction compensation is designed, employing an enhanced linear parameterisation expression. This approach aims to improve parametric estimation accuracy by minimising distortion in the linearity model. On the other side, different from the methods in previous research, by reconfiguring the fast subsystem into a tracking system, i.e. making the real elastic torque track the desired elastic torque, the elastic torque error tends to zero and is not explicitly expressed in the fast subsystem, which allows for greater flexibility in the design of control strategy for the fast subsystem [9, 10, 20]. Additionally, the Lyapunov theorem is utilised to demonstrate that the entire control system is asymptotically stable.

The remains are structured as follows: Section 2 provides the dynamics of the flexible-joint space manipulators and the friction model parameters. In Section 3, the dynamic system of space manipulators with flexible joint is decomposed into two second-order subsystems with distinct time scales utilising singular perturbation theory. Next, an adaptive controller is designed in Section 4, which is followed by the stability proof according to the Lyapunov stability theorem of the provided control strategy in Section 5. In Section 6, numerical simulations and comparable analysis for a 3-linked flexible joint space manipulator are presented. Finally, Section 7 provides conclusions, while Section 8 outlines the future work.

2.0 Dynamic Modeling

The following describes the established dynamic model of a space manipulator with flexible joint: [21, 22]

$$H_l(q)\ddot{q} + C(q,\dot{q})\dot{q} = \tau \tag{1}$$

$$H_m\ddot{\theta} + \tau + \tau_{fr} = \tau_m \tag{2}$$

$$\tau = K(\theta - q) \tag{3}$$

$H_l(q)$ and $C(q,\dot{q})$ are substituted with H_l and C, respectively, to simplify the formulations.

According to various space studies conducted thus far, joint friction appears to be more pronounced in space than on Earth. In this paper, for analytical ease and without sacrificing generality, the mathematical model of joint non-linear friction τ_{fr} takes the form [23–25].

$$\tau_{fr} = B_i\dot{q}_i + [F_{ci} + F_{si}\exp(-F_{\tau i}\dot{q}_i^2)]sign(\dot{q}_i) + F_{ui}(q_i,\dot{q}_i) \tag{4}$$

For the i joint, where $q_i \in R^n$ and $\dot{q}_i \in R^n$ represent the position and velocity of the link, B_i denotes the viscous friction coefficient, F_{ci} symbolises the Coulomb friction-related parameter, F_{si} represents the static friction-related parameter, $F_{\tau i}$ is a positive parameter corresponding to the Stribeck effect, $F_{ui}(q_i,\dot{q}_i)$ captures the position dependency of friction and various friction modeling errors.

https://doi.org/10.1017/aer.2025.10042 Published online by Cambridge University Press

$\hat{B}_i$, $\hat{F}_{ci}$, $\hat{F}_{si}$ and $\hat{F}_{\tau i}$ represent the nominal values of B_i, F_{ci}, F_{si} and $F_{\tau i}$, respectively. The definition of the sign function is

$$sign(\dot{q}_i) = \begin{cases} +1 & \dot{q}_i > 0 \\ 0 & \dot{q}_i = 0 \\ -1 & \dot{q}_i < 0 \end{cases} \tag{5}$$

Under the assumption that the nominal values of $\hat{F}_{si}$ and $\hat{F}_{\tau i}$ are nearly true to their true values, the nonlinear term $F_{si}\exp(-F_{\tau i}\dot{q}_i^2)$ is linearised at $\hat{F}_{si}$ and $\hat{F}_{\tau i}$. Neglecting higher-order terms, the following equation is obtained.

$$\begin{aligned} F_{si}\exp(-F_{\tau i}\dot{q}_i^2) &\cong (\hat{F}_{si}+\tilde{F}_{si})(\exp(-\hat{F}_{\tau i}\dot{q}_i^2) - \exp(-\hat{F}_{\tau i}\dot{q}_i^2)\tilde{F}_{\tau i}\dot{q}_i^2) \\ &\cong \hat{F}_{si}\exp(-\hat{F}_{\tau i}\dot{q}_i^2) + \exp(-\hat{F}_{\tau i}\dot{q}_i^2)\tilde{F}_{si} - \hat{F}_{si}\exp(-\hat{F}_{\tau i}\dot{q}_i^2)\tilde{F}_{\tau i}\dot{q}_i^2) \end{aligned} \tag{6}$$

The linear parameterised friction model can be obtained as follows:

$$\tau_{fri} = B_i\dot{q}_i + [F_{ci} + \hat{F}_{si}\exp(-\hat{F}_{\tau i}\dot{q}_i^2) + \exp(-\hat{F}_{\tau i}\dot{q}_i^2)\tilde{F}_{si} - \hat{F}_{si}\exp(-\hat{F}_{\tau i}\dot{q}_i^2)\tilde{F}_{\tau i}\dot{q}_i^2)]sign(\dot{q}_i) + F_{ui}(q_i, \dot{q}_i) \tag{7}$$

The following is a summary of several characteristics of the manipulator's dynamic model as described in (1), (2) and (3) [8].

Property 1: *$\dot{H}_l(q) - 2C(q,\dot{q})$ is skew-symmetric, satisfying the relationship: $\zeta^T[\dot{H}_l(q) - 2C(q,\dot{q})]\zeta = 0$, $\forall \zeta, q, \dot{q} \in R^n$.*

Property 2: *The inertia matrix $H_l(q)$ is symmetric and positive-definite.*

Property 3: *The Euler-Lagrange dynamics can be expressed in a linearly parameterisable form such that:*

$$H_l(q)\ddot{q} + C(q,\dot{q})\dot{q} = Y(q,\dot{q},\ddot{q})P \tag{8}$$

where $P \in R^r$ is the vector of manipulator parameters, and $Y(q,\dot{q},\ddot{q})$ is a known regressor matrix.

3.0 Two-time Scale Decomposition

Applying singular perturbation decoupling, the dynamic model of the flexible-joint space manipulators described in (1), (2) and (3) can be decomposed into two subsystems with distinct time scales. The manipulator discussed in this section has weak flexibility at the joint, that is, the stiffness coefficient K of the joint is large enough.

All the stiffness coefficients k_i are expressed as a large enough parameter k, provided that they are all of the same order of magnitude [9].

$$K_i = k\tilde{K}_i, i = 1, \cdots, n. \tag{9}$$

$\tilde{K} = diag\left\{\tilde{k}_1, \ldots, \tilde{k}_n\right\}$, to simplify the expression without losing generality, $\tilde{K} = I$.

Equation is derived by substituting equation (3) into the deformed equation (1).

$$\ddot{q} = -H_l^{-1}C\dot{q} + H_l^{-1}\tau \tag{10}$$

Introducing a minimal parameter $\mu = 1/k$, transforming (2) and (9), and then bringing them into (3), equation (11) is obtained.

$$\mu\ddot{\tau} = H_l^{-1}C\dot{q} + H_m^{-1}\tau_m - (H_m^{-1} + H_l^{-1})\tau - H_m^{-1}\tau_{fr} \tag{11}$$

The coupled nonlinear system represented by equations (10) and (11) is the singular perturbation system model. Without simplification, it is unlikely to be tractable for analysis or control-system design [9].

https://doi.org/10.1017/aer.2025.10042 Published online by Cambridge University Press

Employing the notion of integral manifold, the elastic torques τ is defined as following formula,

$$\tau = h(q, \dot{q}, \mu, \tau_m) \tag{12}$$

To simplify the expressions, $h(q, \dot{q}, \mu, \tau_m)$ is substituted with h. Suppose that h is a sufficiently smooth function with regard to the variables q, $\dot{q}$, μ and τ_m. Expanding τ in power series,

$$\tau = h_0 + \mu h_1 + \mu^2 h_2 + \cdots + \mu^n h_n + \cdots \tag{13}$$

where h_0 represents the desired elastic torque, h_i is an expansion of μ, which can be computed iteratively.

Similarly, τ_m expands as follows:

$$\tau_m = \tau_0 + \mu \tau_1 + \mu^2 \tau_2 + \cdots + \mu^n \tau_n + \cdots \tag{14}$$

where τ_0 represents slow subsystem control input torque, namely τ_s.

3.1 Slow subsystem

Observe that, $\mu \to 0$, i.e. $k \to \infty$ will lead to $\theta \to q$ and $\tau \to h_0$, thus the control torque τ_m becomes the slow control law τ_s. Equations (10) and (11) can be expressed as

$$\ddot{q} = -H_l^{-1} C\dot{q} + H_l^{-1} h_0 \tag{15}$$

$$h_0 = (H_m^{-1} + H_l^{-1})^{-1}(H_l^{-1} C\dot{q} + H_m^{-1}\tau_s - H_m^{-1}\tau_{fr}) \tag{16}$$

Substituting equation (16) into equation (15), the slow subsystem is derived as:

$$(H_m + H_l)\ddot{q} + C\dot{q} + \tau_{fr} = \tau_s \tag{17}$$

where τ_s is the slow control input. This subsystem evolves on a time scale $t_{slow} = O(1)$, determined by the perturbation parameter $\mu = 1/k$. For $\mu = 10^4$, τ_f=10^{-4}, implying that the slow dynamics dominate below frequencies $\omega_s = O(1/t_{slow}) \approx 1 rad/s$. Equation (17) represents the rigid part of the dynamics for a flexible-joint space manipulator, which is practically equal to the model of a rigid manipulator. This equivalence allows for leveraging established control strategies from rigid space manipulators to address the challenges posed by the flexible joint manipulators' slow dynamics.

3.2 Fast subsystem

The small enough perturbation coefficient μ has its selection rule dependent on K. K needs to be sufficiently large to guarantee that the fast variable is fast enough on a fast time scale $\mu^{-1}\mathbf{t}$. However, in practice, K cannot approach infinity and typically has an order of magnitude around 10^4, i.e. μ has a value of 10^{-4}. In other words, although μ is minimal, it cannot be infinitely close to zero. Consequently, ignoring the higher-order term of the h will result in an error, necessitating the implementation of a controller within the fast subsystem to restrain the errors resulting from not taking higher-order terms into account.

Considering the neglected higher-order term of the Taylor series expansion for μ in (13) (used to characterise the flexibility factor in the joint), defining the elastic torque error as

$$\eta = h_0 - \tau \tag{18}$$

when $h \to h_0$, $\tau_m \to \tau_s$, equation (11) can be expressed as

$$\mu\ddot{h}_0 = H_l^{-1} C\dot{q} + H_m^{-1}\tau_s - (H_m^{-1} + H_l^{-1})h_0 - H_m^{-1}\tau_{fr} \tag{19}$$

From equations (11), (18) and (19), the fast subsystem can be derived.

$$\mu\ddot{\eta} = -(H_m^{-1} + H_l^{-1})\eta - H_m^{-1}\tau_s \tag{20}$$

https://doi.org/10.1017/aer.2025.10042 Published online by Cambridge University Press

Considering equations (18) and (19), equation (20) can be represented as a refactored fast subsystem

$$\mu\ddot{\tau} = -H_m{}^{-1}\tau_f^* - (H_m{}^{-1} + H_l{}^{-1})\tau \tag{21}$$

where τ_f^* symbolises the control input torque of the refactored fast subsystem, and the interconnection between τ_f^* and τ_f is provided as follows:

$$\tau_f^* = -\mu H_m\ddot{h}_0 - H_m(H_m{}^{-1} + H_l{}^{-1})h_0 - \tau_f \tag{22}$$

It's remarkable that the refactored fast subsystem (21) with a new control objective to control τ tracking h_0 as opposed to (22), which requires the computation of the elastic moment η and its second-order derivative term $\ddot{\eta}$. In other words, the reconfigured fast system controls the fast variable η to converge to zero over time without considering it in the system model. This approach makes the design of the fast subsystem more flexible.

3.3 Corrective control term

It is well known that the conventional singular perturbation method is limited to be utilised in space manipulators with weak joint flexibility. Thus, a corrective control law is derived by comparing the equations of the manipulator system with integral flow to those of a fully rigid manipulator. This comparison yields a new control law design architecture that compensates for flexibility and improves system stiffness. Consequently, this corrective approach extends the applicability of the singular perturbation method to manipulators with strong joint flexibility.

Equation (23) is derived by substituting equations (13) and (14) into the equation (11)

$$\begin{aligned}&\mu(\ddot{h}_0 + \mu\ddot{h}_1 + \mu^2\ddot{h}_2 + \cdots + \mu^n\ddot{h}_n + \cdots)\\ &= H_l{}^{-1}C\dot{q} + H_m{}^{-1}(\tau_0 + \mu\tau_1 + \cdots + \mu^n\tau_n + \cdots)\\ &-(H_m{}^{-1} + H_l{}^{-1})(h_0 + \mu h_1 + \cdots + \mu^n h_n + \cdots) - H_m{}^{-1}\tau_{fr}\end{aligned} \tag{23}$$

Observing the equation (23), the following conclusions in terms of μ can be obtained.

$$0 = H_l{}^{-1}C\dot{q} + H_m{}^{-1}\tau_0 - (H_m{}^{-1} + H_l{}^{-1})h_0 - H_m{}^{-1}\tau_{fr} \tag{24}$$

$$\ddot{h}_{n-1} = H_m{}^{-1}\tau_n - (H_m{}^{-1} + H_l{}^{-1})h_n \tag{25}$$

Considering that the perturbation coefficient μ is small enough, equations (13) and (14) can be rewritten as

$$\tau = h_0 + \mu h_1 \tag{26}$$

$$\tau_m = \tau_0 + \mu\tau_1 = \bar{\tau}_s \tag{27}$$

where τ_1 represents the corrective control term and $\bar{\tau}_s$ represents the corrective slow subsystem control input torque.

Considering equations (24), (25), (26) and (27), equation (10) can be rewritten as

$$\begin{aligned}\ddot{q} = &(-H_l{}^{-1}C + H_l{}^{-1}(H_l{}^{-1} + H_m{}^{-1})^{-1}H_l{}^{-1}C)\dot{q} - (H_l{}^{-1}(H_l{}^{-1} + H_m{}^{-1})^{-1}H_m{}^{-1})\tau_{fr}\\ &-H_l{}^{-1}(H_l{}^{-1} + H_m{}^{-1})^{-1}H_m{}^{-1}\tau_0 + \mu H_l{}^{-1}(H_l{}^{-1} + H_m{}^{-1})^{-1}(H_m{}^{-1}\tau_1 - \ddot{h}_0)\end{aligned} \tag{28}$$

Meanwhile, the corrective fast subsystem control input torque $\bar{\tau}_f$ can be derived by employing equations (14) and (27)

$$\bar{\tau}_f = \mu^2\tau_2 + \cdots + \mu^n\tau_n + \cdots \tag{29}$$

Similar to the fast subsystem described in the section 3.2, the corrected fast subsystem equation for the flexible joint space manipulator with strong joint flexibility can be expressed as follows:

$$\mu\ddot{\tau} = -H_m{}^{-1}\bar{\tau}_f^* - (H_m{}^{-1} + H_l{}^{-1})\bar{\tau} \tag{30}$$

https://doi.org/10.1017/aer.2025.10042 Published online by Cambridge University Press

where $\bar{\tau}_f^*$ symbolises the corrective control input torque of the refactored fast subsystem, and the interconnection between $\bar{\tau}_f^*$ and $\bar{\tau}_f$ is provided as follows:

$$\bar{\tau}_f^* = -\mu H_m \ddot{h}_0 - H_m(H_m{}^{-1} + H_l{}^{-1})h_0 - \bar{\tau}_f - \mu\tau_1 \tag{31}$$

As previously mentioned, for the nonlinear flexible joint space manipulator with strong joint flexibility, the dynamics can be decoupled using singular perturbation theory into the corrected slow subsystem equation (28) and the corrected fast subsystem equations (30) and (31).

It is widely accepted that a rigid space manipulator system can be described in the following general form:

$$H_{lr}(q)\ddot{q} + C_r(q,\dot{q})\dot{q} = \tau_r \tag{32}$$

where H_{lr}, C_r, and τ_r are equivalent to H_l, C, and τ in Section 2. The equation can be represented as:

$$\ddot{q} = -H_{lr}{}^{-1}C_r\dot{q} + H_{lr}{}^{-1}\tau_r \tag{33}$$

To ensure that the stiffness of the manipulator system remains sufficiently large after introducing the corrective control term, it is necessary to make the corrected slow subsystem equation (28) in a flexible joint space manipulator with strong joint flexibility as consistent as possible with the equation (33). Hence, the primary function of the corrective control term (34) is to eliminate all relevant terms in equation (28) with respect to μ.

$$\tau_1 = H_m\ddot{h}_0 \tag{34}$$

4.0 Design of Controller

The fast-slow two-time scale system that is previously presented is obtained by combining the concepts of integral manifolds with singular perturbation theory. The controller design is rendered simplified by this decoupling treatment of the flexible-joint space manipulator's initial complicated dynamics, permitting separate design and implementation of the sub-controllers for each subsystem.

4.1 Control objective

To ensure precise tracking of the desired trajectory and to effectively mitigate vibrations in flexible joints, the implementation of an appropriate control strategy is crucial. Considering joint friction which can disturb the tracking control, an adaptive control approach with friction compensation to guarantee accurate tracking of positions is proposed.

It is assumed that desired trajectory $q_d(t) \in R^n$ is twice differentiable and that $q_d(t)$ and its first two derivatives are bounded for all $t \geq 0$. The control goal of this section is to propose a controller to ensure that the practical trajectory $q(t) \in R^n$ can asymptotically converge to the desired trajectory $q_d(t)$. The trajectory tracking error is described as $e = q - q_d$, the following is the control objective:

$$\forall e(0) \in R^n, \lim_{t\to\infty} e = 0 \tag{35}$$

4.2 Slow subsystem controller

To ensure asymptotic convergence of the tracking and eliminate undesirable steady-state position errors, errors are restricted to lie on a sliding surface [8]

$$\dot{e} + \Lambda e = 0 \tag{36}$$

where the matrix $\Lambda \in R^{n\times n}$ is constant and its eigenvalues are only found on the complex plane's right side. Formally, the goal is achieved by substituting the virtual desired trajectory for $q_d(t)$ in the previous

https://doi.org/10.1017/aer.2025.10042 Published online by Cambridge University Press

derivation

$$q_r = q_d - \Lambda \int_0^t e dt \tag{37}$$

The following definitions are established for the control design:

$$\dot{q}_r = \dot{q}_d - \Lambda e \tag{38}$$

$$\ddot{q}_r = \ddot{q}_d - \Lambda \dot{e} \tag{39}$$

$$s = \dot{q} - \dot{q}_r = \dot{e} + \Lambda e \tag{40}$$

In general, the slow subsystem linearisation is approximated utilising a parameter linearisation method as for rigid manipulators, which is proposed by Slotine and Li [8]. However, this method deteriorates the accuracy of the system parameter estimation and introduces modeling error [26]. An enhanced parameter linearisation method is used in the provided control approach to make the approximation more accurate [27].

$$H_l(\ddot{q}_r + \lambda_c s) + C(\dot{q}_r) = Y(q, \dot{q}, \dot{q}_r, \ddot{q}_r + \lambda_c s)P \tag{41}$$

$$\hat{H}_l(\ddot{q}_r + \lambda_c s) + \hat{C}(\dot{q}_r) = Y(q, \dot{q}, \dot{q}_r, \ddot{q}_r + \lambda_c s)\hat{P} \tag{42}$$

where Y is corresponding regressor matrix, $\hat{P}$ is the approximation of the manipulator parameter P, $\hat{H}_l$ and $\hat{C}$ denote the approximation of H_l and C, λ_c is an arbitrary positive constant.

An adaptive controller for the manipulator with weak joint flexibility is proposed as

$$\tau_s = (\hat{H}_l + \hat{H}_m)(\ddot{q}_r + \lambda_c s) + \hat{C}(\dot{q}_r) - Ks + F \tag{43}$$

where $K = \lambda_c(M + J) + K_s$, of which Ks is positive-definite, and F denotes the friction compensation term.

Define $\tilde{(\cdot)} = \hat{(\cdot)} - (\cdot)$, $(\cdot)$ represents the practical value, $\hat{(\cdot)}$ denotes the approximate value and $\tilde{(\cdot)}$ symbolises the approximation error.

The adaptive control law is proposed as

$$\dot{\hat{P}} = -\Gamma^{-1}(Y^T(q, \dot{q}, \dot{q}_r, \ddot{q}_r + \lambda_c s)s + \Gamma\tilde{P}) \tag{44}$$

where $\Gamma \in R^{n\times n}$ is a positive-definite constant gain matrix.

Moreover, for manipulators with strong joint flexibility, a corrected control term is proposed to improve system stiffness, enabling the control system to manage joint flexibility more effectively. Employing equations, and, the corrective slow subsystem controller is proposed as

$$\bar{\tau}_s = \tau_0 + \mu\tau_1 = (\hat{H}_l + \hat{H}_m)(\ddot{q}_r + \lambda_c s) + \hat{C}(\dot{q}_r) - Ks + F + \mu H_m \ddot{h}_0 \tag{45}$$

4.3 Friction compensator

According to the friction model of the i joint as equation (4), a decomposition-based compensation scheme is applied to design the friction compensator [28]. Where $Z(\dot{q}_i)$ and ${}^i\tilde{F}$ are defined as:

$$Z(\dot{q}_i) = [\dot{q}_i \quad sign(\dot{q}_i) \quad \exp(-\hat{F}_{\tau i}\dot{q}_i^2)sign(\dot{q}_i) \quad -\hat{F}_s\dot{q}_i^2 \exp(-\hat{F}_{\tau i}\dot{q}_i^2)sign(\dot{q}_i)] \tag{46}$$

$${}^i\tilde{F} = [\hat{B}_i - B \quad \hat{F}_c - F_c \quad \hat{F}_s - F_s \quad \hat{F}_\tau - F_\tau] \tag{47}$$

which ${}^i\tilde{F}$ is parametric uncertainty. $\hat{B}_i$, $\hat{F}_c$, $\hat{F}_s$, $\hat{F}_\tau$ are the B_i, F_c, F_s, F_τ nominal values, respectively. In space, the parameter uncertainty caused by huge temperature difference and bad vacuum environment is not always constant. Hence, in order to compensate for its variable parameter uncertainty, the ${}^i\tilde{F}$ representing parameter uncertainty is decomposed:

$${}^i\tilde{F} = {}^i\tilde{F}_c + {}^i\tilde{F}_v \tag{48}$$

https://doi.org/10.1017/aer.2025.10042 Published online by Cambridge University Press

where ${}^i\tilde{F}_c$ is constant but uncertain, and ${}^i\tilde{F}_v$ is variable but bounded:

$$\left|{}^i\tilde{F}_{vn}\right| \le {}^i\delta_{vn} n = 1, 2, 3, 4 \tag{49}$$

Employing the decomposition-based compensation scheme, an integral adaptive compensator u_{pc}^i is proposed with regard to ${}^i\tilde{F}_c$, and a robust compensator u_{pv}^i for ${}^i\tilde{F}_v$. A robust controller u_u^i is intended to compensate the non-parametric uncertainty $F_{ui}(q_i, \dot{q}_i)$. The overall compensation scheme is achieved by combining adaptive and robust compensators, which work together to address the effects of model uncertainties. u_{pc}^i, u_{pv}^i and u_u^i are defined as:

$$u_{pc}^i = -h_1 \int_0^t Z(\dot{q}_i)^T s_i d\tau \tag{50}$$

$$u_{pv(n)}^i = \begin{cases} -{}^i\delta_{vn} \frac{\zeta_n^i}{|\zeta_n^i|} \left|\zeta_n^i\right| > \varepsilon_{pvn}^i \\ -{}^i\delta_{vn} \frac{\zeta_n^i}{\varepsilon_{pvn}^i} \left|\zeta_n^i\right| \le \varepsilon_{pvn}^i \end{cases} n = 1, 2, 3, 4 \tag{51}$$

$$u_u^i = \begin{cases} -\rho_{fi} \frac{s_i}{|s_i|} |s_i| > \varepsilon^i \\ -\rho_{fi} \frac{s_i}{\varepsilon^i} |s_i| \le \varepsilon^i \end{cases} \tag{52}$$

where h_i is a constant, $\zeta_n^i = Z(\dot{q}_i)^T s_i$, ε_{pvn}^i, ε^i are positive control parameters. ρ_{fi} is the upper bound of $F_{ui}(q_i, \dot{q}_i)$, meaning $|F_{ui}(q_i, \dot{q}_i)| < \rho_{fi}$.

For stabilising the joints, the friction compensation term is determined as:

$$F_i = \hat{B}_i \dot{q}_i + [\hat{F}_{ci} + \hat{F}_{si} \exp(-\hat{F}_{\tau i} \dot{q}_i^2)] sign(\dot{q}_i) + Z(\dot{q}_i)(u_{pc}^i + u_{pv}^i) + u_u^i \tag{53}$$

4.4 Fast subsystem controller

The development of the fast subsystem control method focuses on the suppression of vibration of flexible joints, for this reason, many scholars have designed Proportional (P) and PD controllers with torque-feedback based on the information of torque sensors, which are capable of suppressing the vibration of the joints, but cannot take into account the trajectory tracking accuracy at the same time. To address this issue, a new fast subsystem equation (21) is obtained by deforming the fast subsystem equation (20), and the physical meaning of the original fast subsystem is transformed into a typical target tracking problem, that is, the tracking problem of the actual elastic torque to the desired elastic torque.

This section proposed the refactored fast subsystem controller for the manipulator with weak joint flexibility as

$$\tau_f^* = -\mu H_m(\ddot{h}_0 + a_1 \eta + a_2 \dot{\eta}) - H_m({H_m}^{-1} + {H_l}^{-1})\tau \tag{54}$$

where both $a_1 \in R^{n \times n}$ and $a_2 \in R^{n \times n}$ are constant norm-diagonal matrices.

Substituting equation (54) into equation (22), the fast subsystem controller for the manipulator with weak joint flexibility can be obtained.

$$\tau_f = A_1 \eta + A_2 \dot{\eta} \tag{55}$$

where $A_1 = H_m \mu a_1 - H_m({H_m}^{-1} + {H_l}^{-1})$, $A_2 = H_m \mu a_2$.

The fast subsystem's primary objective is to control the elastic torque τ to track h_0, which can be seen as an additional fine-tuning of the slow subsystem control input u_s. Observe that, $A1$ in equation (55) is time-varying, which appears to complicate the control scheme. However, given that M is bounded and the sensitivity of the corresponding boundary value of $A1$ to control performance is limited, an appropriate constant matrix can be chosen simplify the development of the controller. This choice ensures the asymptotic stability of the fast subsystem and simplifies the design of the controller.

https://doi.org/10.1017/aer.2025.10042 Published online by Cambridge University Press

Furthermore, for a manipulator with strong joint flexibility, the corrective controller of the refactored fast subsystem can be derived according to Section 3.3

$$\bar{\tau}_f^* = -\mu H_m(2\ddot{h}_0 + \bar{a}_1\eta + \bar{a}_2\dot{\eta}) - H_m({H_m}^{-1} + {H_l}^{-1})\tau \tag{56}$$

where both $\bar{a}_1 \in R^{n\times n}$ and $\bar{a}_2 \in R^{n\times n}$ are constant norm-diagonal matrices.

Employing equation (31) and (56), the corrective fast subsystem controller for the manipulator with strong joint flexibility can be derived.

$$\bar{\tau}_f = \bar{A}_1\eta + \bar{A}_2\dot{\eta} \tag{57}$$

where $\bar{A}_1 = H_m\mu\bar{a}_1 - H_m({H_m}^{-1} + {H_l}^{-1})$, $\bar{A}_2 = H_m\mu\bar{a}_2$.

Equation (58) are found by substituting equation (54) into equation (21)

$$\ddot{\eta} + a_1\eta + a_2\dot{\eta} = 0 \tag{58}$$

This equation serves as a key component for the stability analysis to be presented later.

4.5 Approximate differential filter

Recalling the provided controller of the space manipulator with various degrees of joint flexibility, the composite control law involves the velocity signal of the links and the differential signal of the joint elastic torque. This section proposes an approximate differential filter to estimate the velocity signal of the links and the differential of the joint elastic torque. This approach avoids noise contamination from measuring the velocity signal and from the numerical differentiation of the elastic torque signal. Ultimately, this approach transforms the full-state closed-loop control into output feedback control based on the position of the links q (measured using a position sensor) and the elastic torque of the joints τ (measured using a joint torque sensor).

The filter is realised for implementation as

$$\dot{\varphi} = -W_1\varphi - W_1W_2u \tag{59}$$

Namely,

$$v = \varphi + W_2u \tag{60}$$

$$\dot{v} = -W_1v + W_2\dot{u} \tag{61}$$

where $v \in R^n$ represents the approximate differential signal, u represents the input signal $(q,\ \tau)$, φ represents an introduced auxiliary variable. $W_1 = diag\{w_{11}, w_{12}, \cdots, w_{1n}\} \in R^{n\times n} W_2 = diag\{w_{21}, w_{22}, \cdots, w_{2n}\} \in R^{n\times n}$, w_{1i} and w_{2i} are positive constants. The filter parameters are all chosen to be positive constants, which ensures the asymptotic stabilisation of the system [32]. The filter (61) is utilised to estimate $\dot{q}, \dot{\tau}$ based on q, τ, resulting in v_q, v_τ.

The global dynamics of the n-DOF flexible joint space manipulators described in (1), (2) and (3) are decomposed into two subsystems under the singular perturbation framework. The controllers for the slow subsystem (rigid portion) and the fast subsystem (flexible portion) are designed separately. The block diagram of the proposed adaptive controller with joint compensation is illustrated in Fig. 2.

5.0 Stability Analysis

For flexible joint space manipulators, control objects can be categorised into the systems with weak joint flexibility and systems with strong joint flexibility based on their joint stiffness coefficients. Accordingly, system stability analysis is also divided into two cases of weak joint flexibility and strong joint flexibility. According to the previous section, the corrective control term τ_1 utilised for equivalent stiffness enhancement in flexible joint space manipulator system with strong joint flexibility is derived from the original fast controller of the manipulator with weak joint flexibility, based on the concept of integral manifold. Therefore, the stability analysis process for systems with weak and strong flexibility is similar. This section only provides the stability analysis of system with weak joint flexibility.

https://doi.org/10.1017/aer.2025.10042 Published online by Cambridge University Press

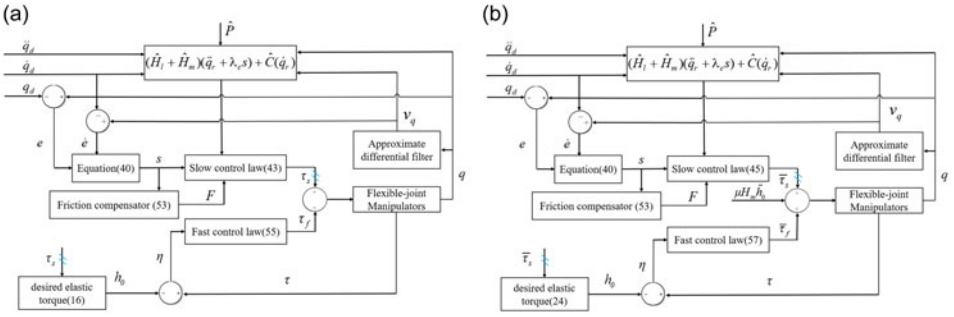


Figure 2. *Structure of the proposed controller for manipulators with weak (a) and strong (b) joint flexibility.*

5.1. Slow subsystem stability analysis

For slow time scale subsystem,

$$V_s = \frac{1}{2}s^T(H_m + H_l)s + \frac{1}{2}h_1\Theta^{\mathbf{T}}\Theta + \frac{1}{2}\tilde{P}^T\Gamma\tilde{P} > 0 \tag{62}$$

where $\Theta = \frac{1}{h_1}\tilde{F}_c - \int_0^t Z(\dot{q})^T s d\tau$, h_1 is a constant and $\dot{\Theta} = -Z(\dot{q})^T s$

Taking the derivative of V_s with regard to time,

$$\begin{aligned}
\dot{V}_s &= s^T(H_m + H_l)\dot{s} + \frac{1}{2}s^T\dot{H}_l s + h_1\Theta^{\mathbf{T}}\dot{\Theta} + \tilde{P}^T\Gamma\dot{\tilde{P}} \\
&= s^T(H_m + H_l)(\ddot{q} - \ddot{q}_r) + \frac{1}{2}s^T\dot{H}_l s + \tilde{P}^T\Gamma\dot{\tilde{P}} - h_1\Theta^{\mathbf{T}}Z(\dot{q})^T s \\
&= s^T[\tau_s - C\dot{q} - \tau_{fr} - (H_m + H_l)\ddot{q}_r)] + \frac{1}{2}s^T\dot{H}_l s + \tilde{P}^T\Gamma\dot{\tilde{P}} - h_1\Theta^{\mathbf{T}}Z(\dot{q})^T s \\
&= s^T[(\hat{H}_l + \hat{H}_m)(\ddot{q}_r + \lambda_c s) + \hat{C}(\dot{q}_r) - \lambda_c(H_m + H_l)s - K_s s + F - C(s + \dot{q}_r) \\
&\quad - \tau_{fr} - (H_m + H_l)\ddot{q}_r)] + \frac{1}{2}s^T\dot{H}_l s + \tilde{P}^T\Gamma\dot{\tilde{P}} - h_1\Theta^{\mathbf{T}}Z(\dot{q})^T s \\
&= s^T(Y\tilde{P} + F - \tau_{fr} - K_s s - Cs) + \frac{1}{2}s^T\dot{H}_l s + \tilde{P}^T\Gamma\dot{\tilde{P}} - h_1\Theta^{\mathbf{T}}Z(\dot{q})^T s \\
&= s^T Y\tilde{P} + \tilde{P}^T\Gamma\dot{\tilde{P}} - s^T K_s s + s^T(F - \tau_{fr}) - h_1\Theta^{\mathbf{T}}Z(\dot{q})^T s \\
&= \tilde{P}^T(Y^T s + \Gamma\dot{\tilde{P}}) - s^T K_s s + s^T(F - \tau_{fr}) - h_1\Theta^{\mathbf{T}}Z(\dot{q})^T s \\
&= -\tilde{P}^T\Gamma\tilde{P} - s^T K_s s + s^T[Z(\dot{q})(\tilde{F}_c + \tilde{F}_v + u_{pc} + u_{pv}) + u_u - F_u(q,\dot{q})] - h_1(\frac{1}{h_1}\tilde{F}_c - \int_0^t Z(\dot{q})^T s d\tau)Z(\dot{q})^T s \\
&= -\tilde{P}^T\Gamma\tilde{P} - s^T K_s s + sZ(\dot{q})^T(\tilde{F}_v + u_{pv}) + s(u_u - F_u(q,\dot{q}))
\end{aligned} \tag{63}$$

Aiming at simplify the analysis, $\dot{V}_s$ is divided as $\dot{V}_s = \dot{V}_1 + \dot{V}_2$, where $\dot{V}_2 = sZ(\dot{q})^T(\tilde{F}_v + u_{pv})$, $\dot{V}_1 = -\tilde{P}^T\Gamma\tilde{P} - s^T K_s s + s(u_u - F_u(q,\dot{q}))$.

When $|s_i| > \varepsilon^i$, combining (52) and (63) yields

$$\begin{aligned}
\dot{V}_1 &= -\tilde{P}^T\Gamma\tilde{P} - s^T K_s s + s(-\rho_f\frac{s}{|s|} - F_u(q,\dot{q})) \\
&= -\tilde{P}^T\Gamma\tilde{P} - s^T K_s s - \rho_f|s| - F_u(q,\dot{q})s \\
&= -\tilde{P}^T\Gamma\tilde{P} - s^T K_s s - |s|(\rho_f - F_u(q,\dot{q})\frac{s}{|s|}) \\
&< -\tilde{P}^T\Gamma\tilde{P} - s^T K_s s
\end{aligned} \tag{64}$$

https://doi.org/10.1017/aer.2025.10042 Published online by Cambridge University Press

When $|s_i| \le \varepsilon^i$

$$\begin{aligned}\dot{V}_1 &= -\tilde{P}^T\Gamma\tilde{P} - s^T K_s s + s(-\rho_f \frac{s}{\varepsilon} - F_u(q,\dot{q})) \\ &= -\tilde{P}^T\Gamma\tilde{P} - s^T K_s s - \frac{\rho_f}{\varepsilon}s^2 - F_u(q,\dot{q})s \\ &\le -\tilde{P}^T\Gamma\tilde{P} - s^T K_s s - \frac{\rho_f}{\varepsilon}s^2 + \rho_f |s|\end{aligned} \tag{65}$$

The term $-(\rho_f/\varepsilon)s^2 + \rho_f |s|$ reaches its maximum value $-\rho_f\varepsilon/4$ when $|s| = \varepsilon/4$. It is evident that

$$\dot{V}_1 \le -\tilde{P}^T\Gamma\tilde{P} - s^T K_s s + \frac{\rho_f \varepsilon}{4} \tag{66}$$

Since

$$sZ(\dot{q})^T(\tilde{F}_v + u_{pv}) = \sum_{n=1}^{4} s_i Z(\dot{q})^T(\tilde{F}_{vn} + u_{pvn}) = \sum_{n=1}^{4} \zeta_n(\tilde{F}_{vn} + u_{pvn}) \tag{67}$$

According to (51) if $\left|\zeta_n^i\right| > \varepsilon_{pvn}^i$, for $n = 1,2,3,4$

$$\zeta_n(\tilde{F}_{vn} + u_{pvn}) = \zeta_n(\tilde{F}_{vn} - \delta_{vn}\frac{\zeta_n}{|\zeta_n|}) < 0 \tag{68}$$

If $\left|\zeta_n^i\right| \le \varepsilon_{pvn}^i$

$$\zeta_n(\tilde{F}_{vn} + u_{pvn}) = \zeta_n(\tilde{F}_{vn} - \delta_{vn}\frac{\zeta_n}{\varepsilon_{pvn}}) \le \zeta_n(\delta_{vn}\frac{\zeta_n}{|\zeta_n|} - \delta_{vn}\frac{\zeta_n}{\varepsilon_{pvn}}) \tag{69}$$

(69) reaches its maximum value $\rho_f\varepsilon/4$ when $|\zeta_n| = \varepsilon_{pvn}/2$. It can be observed that

$$\dot{V}_2 \le \sum_{n=1}^{4} \delta_{vn}\varepsilon_{pvn}/4 \tag{70}$$

Combining the results in (64), (66), (68) and (70), the following inequality can be obtained:

$$\dot{V}_s \le -\tilde{P}^T\Gamma\tilde{P} - s^T K_s s + \frac{\rho_f\varepsilon}{4} + \sum_{n=1}^{4} \delta_{vn}\varepsilon_{pvn}/4 \tag{71}$$

Inequality (71) leads to the conclusion that a Lyapunov function can be located if only

$$|s| \ge \frac{1}{2}\sqrt{\frac{\rho_f\varepsilon + \sum_{n=1}^{4}\delta_{vn}\varepsilon_{pvn}}{K_s}} \tag{72}$$

On the other hand, when

$$|s| < \frac{1}{2}\sqrt{\frac{\rho_f\varepsilon + \sum_{n=1}^{4}\delta_{vn}\varepsilon_{pvn}}{K_s}} \tag{73}$$

Based on the conclusion presented by Slotine and Li [29], $\dot{e}$ and $\dot{e}_i$ are also bounded if s is bounded.

5.2 Fast subsystem stability analysis

For the fast time scale subsystem,

$$V_f = \frac{1}{2}\mu(\dot{\eta}^T\dot{\eta} + \eta^T\dot{\eta} + \eta^T\eta) \tag{74}$$

https://doi.org/10.1017/aer.2025.10042 Published online by Cambridge University Press

Defining $\Omega = (\eta^T, \dot{\eta}^T)^T$, V are rewritten as

$$V_f = \frac{1}{2}\mu\Omega^T H\Omega \geq \frac{1}{2}\mu\lambda_{\min}\{H\}\|\Omega\|^2 \geq 0 \tag{75}$$

where $H = \begin{pmatrix} 1 & 1/2 \\ 1/2 & 1 \end{pmatrix}$.

Taking the derivative of the Lyapunov function candidate V_f with regard to the fast scaled time $\delta = \mathbf{t}/\mu$, and substituting the elastic torque error equation

$$\begin{aligned} \dot{V}_f &= \dot{\eta}^T\ddot{\eta} + \frac{1}{2}\dot{\eta}^T\dot{\eta} + \frac{1}{2}\eta^T\ddot{\eta} + \eta^T\dot{\eta} \\ &= \dot{\eta}^T(-a_1\eta - a_2\dot{\eta}) + \frac{1}{2}\dot{\eta}^T\dot{\eta} + \frac{1}{2}\eta^T(-a_1\eta - a_2\dot{\eta}) + \eta^T\dot{\eta} \\ &= -\dot{\eta}^T a_2\dot{\eta} + \frac{1}{2}\dot{\eta}^T\dot{\eta} - \dot{\eta}^T a_1\eta - \frac{1}{2}\eta^T a_2\dot{\eta} + \eta^T\dot{\eta} - \frac{1}{2}\eta^T a_1\eta \end{aligned} \tag{76}$$

The following inequalities can be established determined by Rayleigh–Ritz inequality [20],

$$\begin{gathered} -\dot{\eta}^T a_2\dot{\eta} \leq -\lambda_{\min}(a_2)\|\dot{\eta}\|^2 \\ \tfrac{1}{2}\dot{\eta}^T\dot{\eta} \leq \tfrac{1}{2}\|\dot{\eta}\|^2 \\ -\dot{\eta}^T a_1\eta \leq -\sigma_{\min}(a_1)\|\dot{\eta}\|\|\eta\| \\ -\tfrac{1}{2}\eta^T a_2\dot{\eta} \leq -\tfrac{1}{2}\sigma_{\min}(a_2)\|\eta\|\|\dot{\eta}\| \\ \eta^T\dot{\eta} \leq \|\eta\|\|\dot{\eta}\| \\ -\tfrac{1}{2}\eta^T a_1\eta \leq -\lambda_{\min}(a_1)\|\eta\|^2 \end{gathered} \tag{77}$$

where $\sigma_{\min}(\cdot)$ and $\lambda_{\min}(\cdot)$ denote the matrix' the minimum singular and minimum eigenvalue value, respectively.

Equation (76) can be expressed as follows by sequentially applying the aforementioned inequalities:

$$\dot{V}_f \leq -T^T QT \tag{78}$$

where

$$T = \begin{pmatrix} \|\dot{\eta}\| \\ \|\eta\| \end{pmatrix}, Q = \begin{pmatrix} \lambda_{\min}(a_2) - \frac{1}{2} & \frac{2\sigma_{\min}(a_1)+\sigma_{\min}(a_2)-2}{4} \\ \frac{2\sigma_{\min}(a_1)+\sigma_{\min}(a_2)-2}{4} & \lambda_{\min}(a_1) \end{pmatrix}$$

In order to guarantee that $\dot{V}_f$ is negative-definite, Q must satisfy the following inequalities so as to be a positive-definite matrix:

$$\lambda_{\min}(a_2) > \frac{1}{2}, (\lambda_{\min}(a_2) - \frac{1}{2})\lambda_{\min}(a_1) - \left(\frac{2\sigma_{\min}(a_1) + \sigma_{\min}(a_2) - 2}{4}\right)^2 > 0 \tag{79}$$

Therefore, if the above condition (79) holds, V_f is positive-definite, $\dot{V}_f$ is negative-definite, the asymptotic stability of fast subsystem can be demonstrated.

5.3 The entire system stability analysis

For the entire system, the Lyapunov function candidate is considered as follows: [20]

$$V = V_s + V_f \tag{80}$$

where *Vs* represents the Lyapunov function candidate for the slow time scale subsystem shown in equation (17) and V_f represents that for the fast time scale subsystem shown in equation (21), and both c_1 and c_2 are positive constants. It is evident from the previous proof that $V = V_s + V_f$ is positive-definite.

https://doi.org/10.1017/aer.2025.10042 Published online by Cambridge University Press

Table 1. *Manipulator's parameters for simulation*

Parameters	Link 1	Link 2	Link 3
Mass (kg)	1.2	1.2	1.2
Link inertia (kg m^2)	0.4	0.4	0.4
Length (m)	1	1	1
Rotor inertia (kgm^2)	5×10^{-6}	5×10^{-6}	5×10^{-6}
Gear ratio *ri*	200	200	200

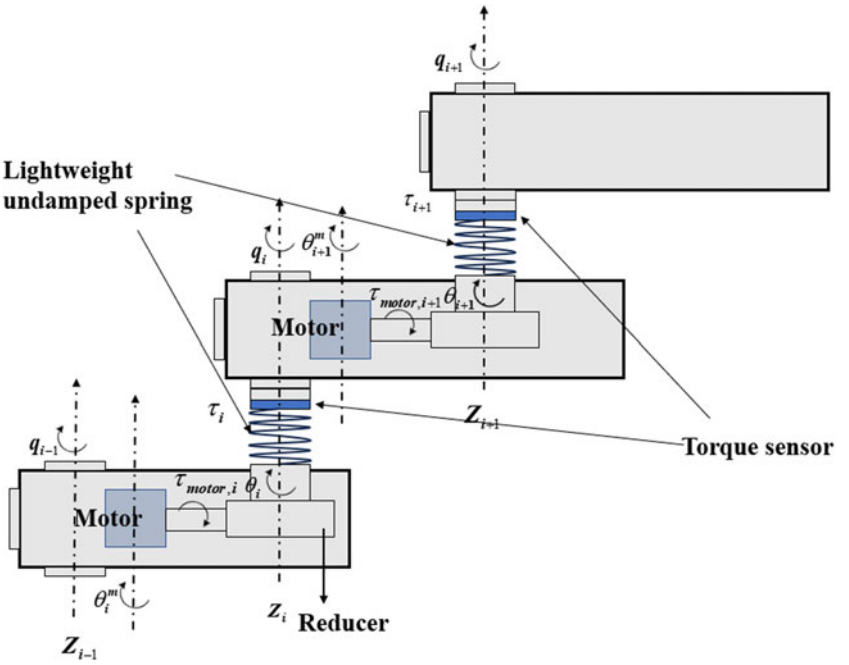


Figure 3. *Simulation model of space manipulator.*

Obviously

$$\dot{V} = \dot{V}_s + \dot{V}_f \tag{81}$$

The stability of the first part of equation is proven using a similar method to that in Section 5.1. It is important to note a key difference: equation (10) is used to replace equation (17) and is then substituted into $\dot{V}_s$, because of the representation of the entire system by equations (10) and (11). The stability proof of the fast time scale subsystem employs the same as approach that described in the previous part. Aa a result, it is determined that $\dot{V}$ is negative definite, leading the conclusion that the entire composite system is asymptotically stable.

6.0 Simulation Results

This section aims to demonstrate the effective performance of the proposed controller by conducting simulations on a three-link flexible-joint space manipulator (Table 1) with different joint stiffnesses and comparing its control effect with that of the traditional adaptive controller (TAC) [30]. The simulation model is shown in Fig. 3.

The following is the expressions for $H_l(q)$, $C(q, \dot{q})$ with respect to the elements of the space manipulator parameters vector P:

https://doi.org/10.1017/aer.2025.10042 Published online by Cambridge University Press

$$H_l(q)=\begin{bmatrix} H_{l11} & H_{l12} & H_{l13} \\ H_{l21} & H_{l22} & H_{l23} \\ H_{l31} & H_{l32} & H_{l33} \end{bmatrix}, C(q,\dot{q})=\begin{bmatrix} C_{11} & C_{12} & C_{13} \\ C_{21} & C_{22} & C_{23} \\ C_{31} & C_{32} & C_{33} \end{bmatrix}, J=diag\{0.2,0.2,0.2\}$$

$$H_{l11}=p_1+p_4+p_5+p_9\cos q_2+2p_7\cos q_2+p_6\cos(q_2+q_3)+p_8\cos q_3$$

$$H_{l12}=H_{l21}=p_2+p_5+0.5p_9\cos q_2+p_8\cos q_3+p_7\cos q_2+0.5p_6\cos(q_2+q_3)$$

$$H_{l13}=H_{l31}=p_3+0.5p_8\cos q_3+0.5p_6\cos(q_2+q_3)$$

$$H_{l22}=p_2+p_5+p_8\cos q_3$$

$$H_{l23}=H_{l32}=p_3+0.5p_8\cos q_3$$

$$H_{l33}=p_3$$

$$C_{11}=-0.5p_9\dot{q}_2\sin(q_2)-0.5p_6\dot{q}_3\sin(q_2+q_3)-0.5p_6\dot{q}_2\sin(q_2+q_3)-p_7\dot{q}_2\sin(q_2)-0.5p_8\dot{q}_3\sin q_3$$

$$C_{12}=-0.5p_9(\dot{q}_1+\dot{q}_2)\sin(q_2)-0.5p_6(\dot{q}_1+\dot{q}_2+\dot{q}_3)\sin(q_2+q_3)-p_7(\dot{q}_1+\dot{q}_2)\sin(q_2)$$

$$C_{13}=-0.5p_8\dot{q}_2\sin q_3-0.5p_6(\dot{q}_1+\dot{q}_2+\dot{q}_3)\sin(q_2+q_3)-0.5p_8(\dot{q}_1+\dot{q}_2+\dot{q}_3)\sin q_3$$

$$C_{21}=0.5p_9\dot{q}_1\sin q_2+0.5p_6\dot{q}_1\sin(q_2+q_3)+p_7\dot{q}_1\sin(q_2)$$

$$C_{22}=-0.5p_8\dot{q}_3\sin q_3$$

$$C_{23}=-0.5p_8\dot{q}_2\sin q_3-0.5p_8\dot{q}_3\sin q_3-p_8\dot{q}_1\sin q_3$$

$$C_{31}=p_8\dot{q}_1\sin q_3+0.5p_8\dot{q}_2\sin q_3$$

$$C_{33}=0$$

$$P=(p_1\quad p_2\quad p_3\quad p_4\quad p_5\quad p_6\quad p_7\quad p_8\quad p_9)^T$$

About the friction compensation F, the parameters for the simulation are set as:

$$B_i=2.5+0.7\sin(10q_i)Nms/rad$$
$$F_{ci}=4.5+0.5\sin(10q_i)Nm$$
$$F_{si}=5+0.7\sin(10q_i)Nm$$
$$F_{\tau i}=100+20\cos(10q_i)s^2/rad^2$$

The following are the uncertainty boundaries and associated parameters:

$$h_1=h_2=h_3=1,\ \varepsilon^i_{pvn}=0.01,\ \varepsilon^i=0.1,\ \rho_{fi}=0.5,\ {}^i\delta_{v1}={}^i\delta_{v3}=0.7,\ {}^i\delta_{v2}=0.5,\ {}^i\delta_{v4}=20$$

The nominal friction parameters of the proposed friction model are as follows:

$$\hat{B}_i=1.8Nms/rad,\ \hat{F}_{ci}=3.6Nm,\ \hat{F}_{si}=4.0Nm,\ \hat{F}_{\tau i}=80s^2/rad^2$$

Position-dependent friction and other friction modeling errors $F_{ui}(q_i,\dot{q}_i)$ in friction models described as $0.5\sin(3q)$.

For simplicity, the same friction model and parameters were selected for all joints. The following is the desired trajectories for three joints:

$$q_{d1}=1/(2\pi)\sin(2\pi t+\pi/2)rad$$
$$q_{d2}=1/(2\pi)\sin(2\pi t+\pi/2)rad$$
$$q_{d3}=1/(2\pi)\sin(2\pi t+\pi/2)rad$$

For a three-link flexible-joint space manipulator (Table 1) with weak joint flexibility, namely K=10,000, simulations were conducted to compare the provided novel adaptive controller (NAC) with the TAC, verifying the effectiveness of the proposed control strategy.

The control law of NAC is presented by equations (43), (44), (53) and (55). The control law of TAC is given by equation (82):

$$\begin{aligned} \tau_s{}' &= (\hat{H}_l+\hat{H}_m)\ddot{q}_r+\hat{C}\dot{q}_r-K_s s+F, \\ \dot{\hat{P}}' &= -\Gamma^{-1}Y^T(q,\dot{q},\dot{q}_r,\ddot{q}_r)s, \\ \tau_f{}' &= A_1\eta+A_2\dot{\eta} \end{aligned} \tag{82}$$

where $\tau_s{}'$ and $\tau_f{}'$ act on the slow and fast subsystem, respectively.

https://doi.org/10.1017/aer.2025.10042 Published online by Cambridge University Press

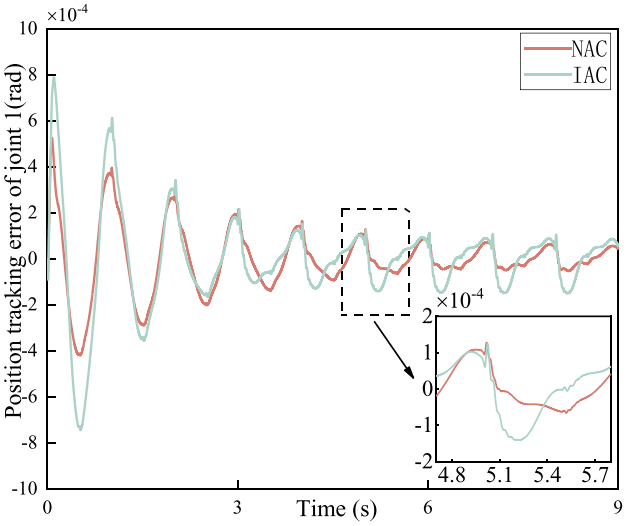


Figure 4. *Tracking error of joint 1(K = 10,000).*

After trials and errors, the same parameters for both controllers (TAC, NAC) take the following values:

$$\Gamma = diag\{100, 100, 100, 100, 100, 100, 100, 100, 100\}$$
$$K_s = diag\{600, 600, 600\}, \Lambda = diag\{80, 80, 80\}$$
$$A_1 = diag\{1.5, 1.5, 1.5\}, A_2 = diag\{0.03, 0.03, 0.03\}$$

The standard criteria proposed in [30] were adopted to evaluate the control performance. This represents the average performance with regard to tracking errors.

$$RMS(e_i) = \sqrt{\int_0^T |e_i|^2 \, dt/T}, i = 1, 2, 3 \tag{83}$$

$$RMS(\mathbf{e}) = \sqrt{\int_0^T \|\mathbf{e}\|^2 \, dt/T} \tag{84}$$

Figure 7 illustrates the driving torque of all joints utilising the adaptive control method (NAC) proposed in this paper.

Simultaneously, from the position tracking error curves in Figs 4, 5 and 6, it is evident that the presented adaptive control strategy yields smaller position errors than the traditional that (TAC). The reason for this is that the proposed control approach employs an enhanced linear parameterisation formulation by (41) that improves the estimation accuracy of adaptive parameters. As demonstrated in Table 2, the RMS(e) in the proposed approach (NAC) decreases by 31.8% at the first joint, 27.1% at the second joint, 8.7% at the third joint and 28.1% on the overall compared with these of the controller (TAC), respectively. Furthermore, an approximate differential filter is used to estimate the velocity signal of the links, avoiding noise contamination from measuring the velocity signal directly and improving the robustness of the control system. Typically, the higher the applied torque, the lesser the impact of friction on the variation of joint angle. As can be observed from the Figs 4–6, the effect of friction on the variation of joint angles is more pronounced in joint 3 as compared to joints 1 and 2. However, the jitter in the error curve due to friction is slight, indicating that it is well suppressed by the friction compensator. Simulation results demonstrate that the adaptive controller provided in the paper can well suppress the effects of joint vibration and joint friction on the accurate movements of manipulators.

https://doi.org/10.1017/aer.2025.10042 Published online by Cambridge University Press

Table 2. *Performance comparison (K = 10,000)*

Parameters		NAC	TAC
RMS(e) (rad)	e_1	1.3818×10^{-2}	2.0288×10^{-2}
	e_2	1.4916×10^{-2}	2.0464×10^{-2}
	e_3	4.2771×10^{-2}	8.1859×10^{-2}
	$\|\mathbf{e}\|$	1.69×10^{-2}	2.51×10^{-2}

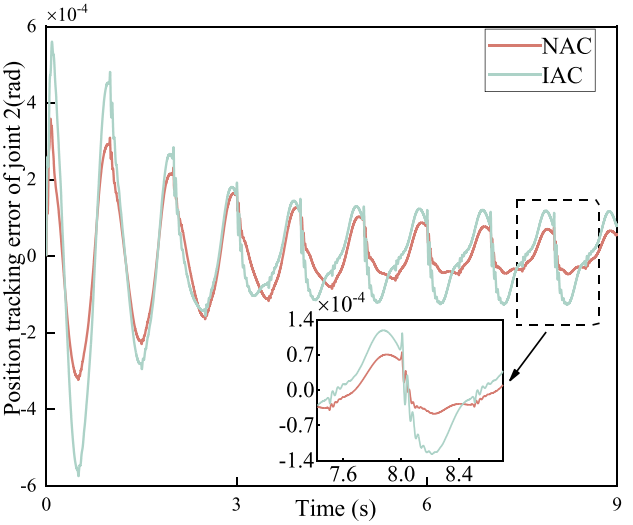


Figure 5. *Tracking error of joint 2(K = 10,000).*

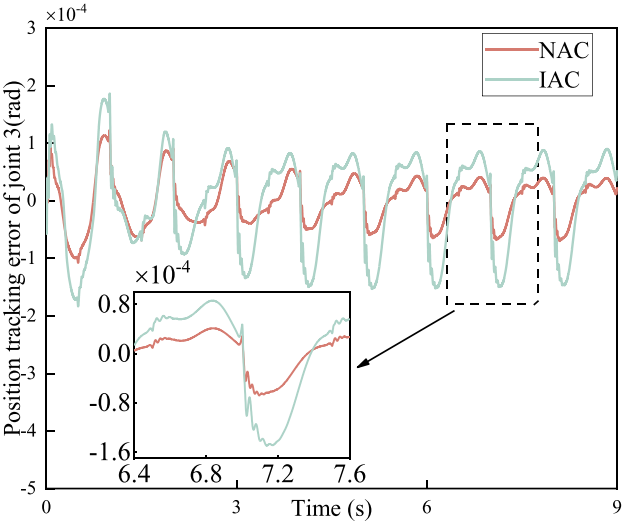


Figure 6. *Tracking error of joint 3(K = 10,000).*

https://doi.org/10.1017/aer.2025.10042 Published online by Cambridge University Press

Table 3. *Performance comparison ($K = 2{,}000$)*

Parameters		NAC + CC	NAC + FC
RMS(e) (rad)	e_1	5.0231×10^{-2}	8.0478×10^{-2}
	e_2	3.841×10^{-2}	6.1552×10^{-2}
	e_3	2.2229×10^{-2}	4.8811×10^{-2}
	$\|\mathbf{e}\|$	4.69×10^{-2}	7.51×10^{-2}

Previous simulation results indicate that the adaptive controller proposed in the paper achieves better trajectory tracking when system stiffness is high (i.e. system with weak joint flexibility). For a manipulator system with strong joint flexibility, to verify the effectiveness and superiority of the corrective control scheme (CC) proposed in Section 3.3, comparative simulations are conducted on the provided NAC with the corrected control term in this paper and the provided NAC with the flexibility compensator (FC) in the literature [31].

The following is a description of the flexibility compensator in the literature [31].

$$\tau_1{}' = K_t\tau,\ \tau_m{}' = K_a(\tau_s{}' + \tau_f{}') + \tau_1{}' \tag{85}$$

where $\tau_m{}'$ represents the composite control input torque, $\tau_1{}'$ represents the flexibility compensation section, K_t and K_a are fixed-parameter matrices. The two matrices satisfy the relationship:$K_a = I + K_t$.

Note that, to validate the effectiveness of the provided NAC + CC, simulations are conducted on the manipulator (Table 1) with different joint stiffness coefficient (namely K=5,000, 2,000 and 800, respectively). After trials and errors, the parameters take the following values:

$$\Gamma = diag\{100, 100, 100, 100, 100, 100, 100, 100, 100\}$$
$$K_s = diag\{300, 300, 300\},\ \Lambda = diag\{80, 80, 80\}$$
$$\bar{A}_1 = diag\{8, 8, 8\},\ \bar{A}_2 = diag\{0.09, 0.09, 0.09\}$$

As shown in Figs 8, 9 and 10, it is clearly noticed that the trajectory tracking error curves of the three joints almost coincide when the stiffness coefficients $K = 5{,}000$ and $K = 2{,}000$, and the absolute value of the error in the steady state remains at the order of 10^{-4}. The results indicate that the calibratable control law can effectively compensate for strong flexibility in the system, and it has excellent adaptability to the systems with different strong flexibility (under different stiffness coefficients, the system controller does not need to change the simulation parameters). However, when the stiffness coefficient $K = 800$, the trajectory tracking error significantly increases in the steady state compared to the first two cases, and the regulation time also increases. This indicates that when the joint flexibility of the system exceeds a certain limit, the proposed correctable control law for flexibility compensation is less effective for enhancing the equivalent system's stiffness. However, it still manages to maintain a good error steady state.

Observe that, for the three-link flexible-joint space manipulator (Table 1) with strong joint flexibility (namely $K = 2{,}000$), simulations are conducted to compare the provided novel adaptive controller with the corrected control term (CC) in this paper and the provided novel adaptive controller with the FC. The parameters for controllers take the following values:

$$\Gamma = diag\{100, 100, 100, 100, 100, 100, 100, 100, 100\}$$
$$K_s = diag\{300, 300, 300\},\ \Lambda = diag\{80, 80, 80\}$$
$$\bar{A}_1 = diag\{8, 8, 8\},\ \bar{A}_2 = diag\{0.09, 0.09, 0.09\}$$
$$K_t = diag\{120, 120, 120\},\ K_a = diag\{121, 121, 121\}$$

Observing Figs 11, 12 and 13, it is evident that both the corrective control law and the flexibility compensator effectively enhance stiffness in the flexible joint space manipulator system with strong joint flexibility, successfully overcoming the vibrations generated at the flexible joints. However,

https://doi.org/10.1017/aer.2025.10042 Published online by Cambridge University Press

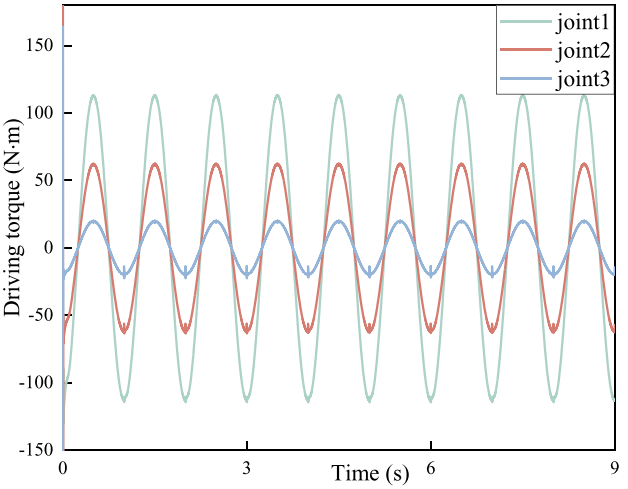


Figure 7. *Driving torque of three joints (NAC).*

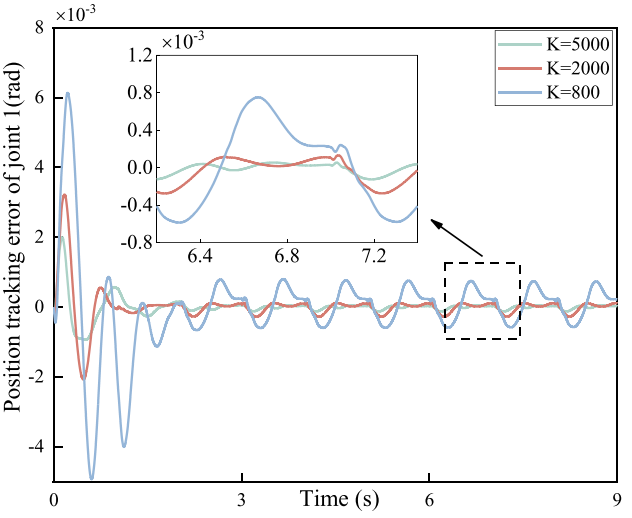


Figure 8. *Tracking error of joint 1.*

the choice of tuning parameters for the latter is constrained by factors such as unmodeled dynamics, sensor noise and signal sampling frequency, preventing the indefinite scaling up of equivalent stiffness [33]. Furthermore, in terms of regulation time and steady-state error value, the former performs slightly better.

7.0 Conclusions

This paper provided a novel adaptive control approach according to singularly perturbed decoupling and integral manifold concept for flexible-joint space manipulators considering parametric uncertainties and joints friction. The control scheme includes a decomposition-based friction compensator, a modified compensation term to enhance system stiffness, and a composite adaptive controller to mitigate joint flexibility. The decomposition-based friction compensation scheme aims to deal with various kinds of

https://doi.org/10.1017/aer.2025.10042 Published online by Cambridge University Press

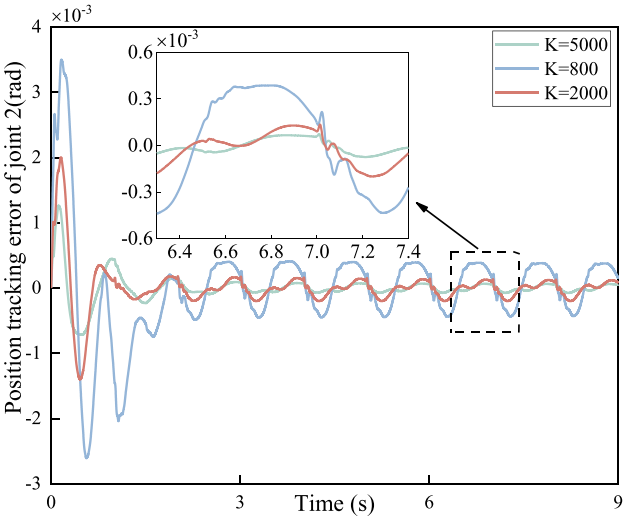


Figure 9. *Tracking error of joint 2.*

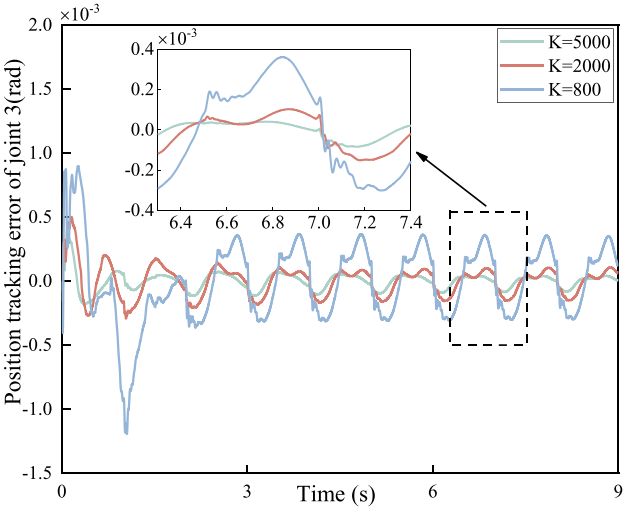


Figure 10. *Tracking error of joint 3.*

model uncertainty in an appropriate way. An adaptive compensator addresses the unknown but constant portion of the variable parametric friction model uncertainty, while a robust compensator manages the variable yet bounded portion. It is emphasised by an enhanced parameter linearisation formulation and an approximate differential filter invoked in the proposed controller. Approximate differential filters are utilised to estimate the joint velocities of the links and the differential terms of joint elastic torques, which reduces noise disturbances and improves the robustness of the control system. Moreover, a modified compensation law is proposed to enhance system stiffness, addressing the limitations of the traditional singular perturbation method, which is only suitable for space manipulators with weak joint flexibility. In addition, the asymptotic stability of the system is proved based on Lyapunov's theory. Finally, simulations presented on a three-degree-of-freedom manipulator are illustrated to examine the performance of the provided control strategy and comparisons with the TAC to verify the superiorities of the provided controller.

https://doi.org/10.1017/aer.2025.10042 Published online by Cambridge University Press

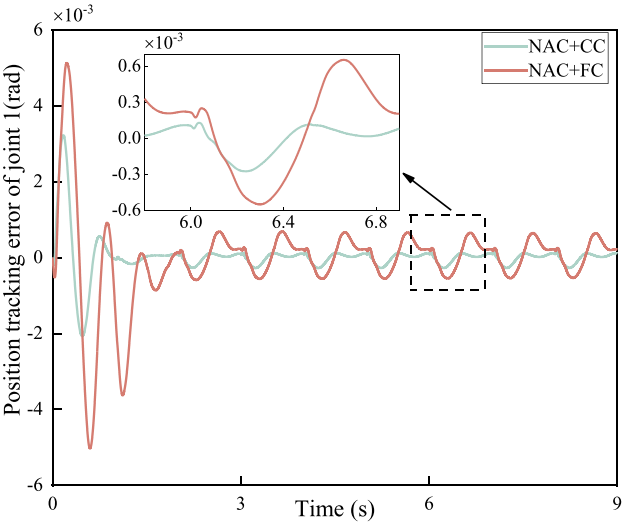


Figure 11. *Tracking error of joint 1(K = 2,000).*

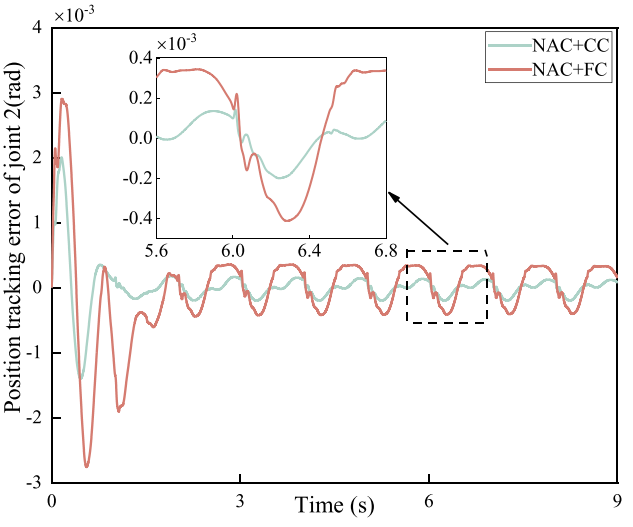


Figure 12. *Tracking error of joint 2(K = 2,000).*

8.0 Future Work

While the proposed adaptive control approach demonstrates promising performance in simulation environments, several avenues remain open for further exploration to advance its theoretical foundations and practical applicability:

Experimental Validation on Physical Platforms: Implementing the controller on a ground-based space manipulator testbed to evaluate its robustness under real-world disturbances. This will bridge the gap between theoretical design and practical deployment.

Multi-Objective Optimisation: Integrating trajectory planning with the adaptive controller to jointly optimise energy efficiency, vibration suppression and tracking accuracy. Techniques such as dynamic programming or reinforcement learning could be explored to address this coupled optimisation problem.

https://doi.org/10.1017/aer.2025.10042 Published online by Cambridge University Press

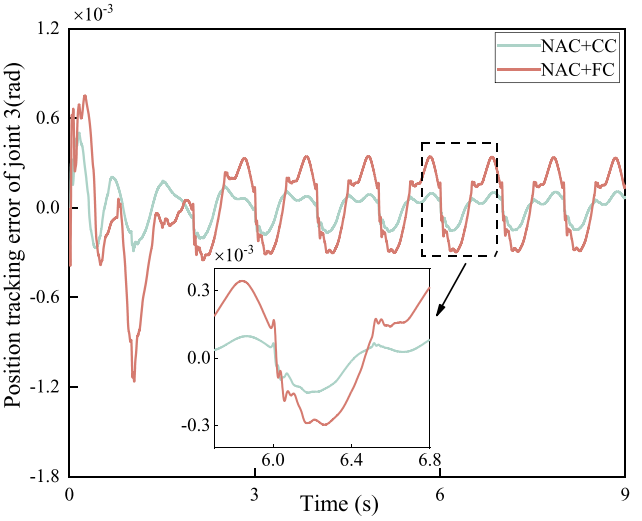


Figure 13. *Tracking error of joint 3(K = 2,000).*

Data-Driven Friction Compensation: Enhancing the friction compensator by incorporating neural networks or Gaussian processes to model unmeasured nonlinearities. Hybrid models combining physics-based and data-driven approaches may further improve compensation accuracy.

Declaration of Competing Interest. The authors declare that they have no known competing financial interests or personal relationships that could have appeared to influence the work reported in this paper.

References

[1] Zhou, Y., Luo, J. and Wang, M. Grasping force optimization for dual-arm space robot after capturing target based on task compatibility, *Adv. Space Res.*, 2022, **70**, pp 1496–1511.
[2] Wei, Z., Long, T., Shi, R. and Song, X. Electric thruster configuration design optimization for geostationary satellites with robotic manipulators, *Adv. Space Res.*, 2022, **69**, pp 3798–3813.
[3] Talole, S.E., Kolhe, J.P. and Phadke, S.B. Extended-state-observer-based control of flexible-joint system with experimental validation, *IEEE Trans. Ind. Electron.*, 2010, **57**, pp 1411–1419.
[4] Rupp, T., Boge, T., Kiehling, R. and Sellmaier, F. Flight Dynamics Challenges of the German On-Orbit Servicing Mission DEOS, In *21st International Symposium on Space Flight Dynamics*, Toulouse, France, 2009.
[5] Jaekel, S., et al., Design and operational elements of the robotic subsystem for the e.deorbit debris removal mission, *Front. Robot. AI*, 2018, **5**, pp 100.
[6] Jin, M., Lee, J. and Tsagarakis, N.G. Model-free robust adaptive control of humanoid robots with flexible joints, *IEEE Trans. Ind. Electron.*, 2017, **64**, pp 1706–1715.
[7] Ma, H., Zhou, Q., Li, H. and Lu, R. Adaptive prescribed performance control of a flexible-joint robotic manipulator with dynamic uncertainties, *IEEE Trans. Cybern.*, 2022, **52**, pp 12905–12915.
[8] Slotine, J.J.E. and Li, W. On the adaptive control of robot manipulators, *Int. J. Rob. Res.*, 1987, **6**, pp 49–59.
[9] Spong, M.W., Khorasani, K. and Kokotovic, P. An integral manifold approach to the feedback control of flexible joint robots, *IEEE J. Robot. Autom.*, 1987, **3**, pp 291–300.
[10] Spong, M.W. Modeling and control of elastic joint robots, *ASME. J. Dyn. Sys., Meas., Control*, 1987, **109**, pp 310–318.
[11] Huang, L., Ge, S.S. and Lee, T.H. Position/force control of uncertain constrained flexible joint robots, *Mechatronics*, 2006, **16**, pp 111–120.
[12] Subudhi, B. and Morris, A.S., Singular Perturbation Approach to Trajectory Tracking of Flexible Robot with Joint Elasticity, *Int. J. Syst. Sci.*, 2003, **34**, pp 167–179.
[13] Zhu, W.H., Dupuis, E. and Doyon, M. Adaptive control of harmonic drives, *ASME. J. Dyn. Sys. Mears. Control*, 2007, **129**, pp 182–193.
[14] Le-Tien, L. and Albu-Schäffer, A. Adaptive friction compensation in trajectory tracking control of DLR medical robots with elastic joints, In *IEEE/RSJ International Conference on Intelligent Robots and Systems*, 2012, vol. 5, pp 1149–1154.
[15] Zhang, Q., Liu, X. and Cai, G. Dynamics and control of a flexible-link flexible-joint space robot with joint friction, *Int. J. Aeronaut. Space Sci.*, 2021, **22**, pp 415–432.

https://doi.org/10.1017/aer.2025.10042 Published online by Cambridge University Press

[16] Wu, Z. Adaptive block compensation trajectory tracking control based on LuGre friction model, *Int. J. Adv. Rob. Syst.*, **16**, 2019.
[17] Zhang, Q., Liu, X. and Cai, G. Dynamics and control of a flexible-link flexible-joint space robot with joint friction, *Int. J. Aeronaut. Space Sci.*, 2021, **22**, pp 415–432.
[18] Zhang, F. and Yuan, Z. The study of coupling dynamics modeling and characteristic analysis for flexible robots with nonlinear and frictional joints, *Arab J Sci Eng.*, 2022, **17**, pp 15347–15363.
[19] Gao, H., Li, Y., Guan, H. and Hao, F. Dynamic simulation of modular robot joint with friction and flexibility, In *CSAE 2020: Proceedings of the 4th International Conference on Computer Science and Application Engineering*, Association for Computing Machinery, 2020, vol. 91, pp 1–5.
[20] Khosravi, M.A. and Taghirad, H.D. Dynamic modeling and control of parallel robots with elastic cables: singular perturbation approach, *IEEE Trans. Robot.*, 2014, **30**, pp 694–704.
[21] Ruderman, M. Compensation of nonlinear torsion in flexible joint robots: comparison of two approaches, *IEEE Trans. Ind. Electron.*, 2016, **63**, pp 5744–5751.
[22] Ulrich, S. and Sasiadek, J.Z. Modeling and direct adaptive control of a flexible-joint manipulator, *J. Guid. Control Dyn.*, 2012, **35**, pp 25–39.
[23] Ahmad, S. Multiple working mode control of door-opening with a mobile modular and reconfigurable robot, *IEEE/ASME Trans. Mechatron.*, 2013, **18**, pp 833–844.
[24] Dong, B., Zhou, F., et al. Decentralized robust optimal control for modular robot manipulators via critic-identifier structure-based adaptive dynamic programming, *Neural Comput & Applic*, 2020, **32**, pp 3441–3458.
[25] Liu, G., Abdul, S. and Goldenberg, A.A. Distributed control of modular and reconfigurable robot with torque sensing, *Robotica*, 2008, **26**, pp 75–84.
[26] Raouf, F., Mohamad, S., Maarouf, S. and Maamar, B. Distributed adaptive control strategy for flexible link manipulators, *Robotica*, 2016, **35**, pp 1562–1584.
[27] Liu, H., Huang, Y. and Wu, W. Improved adaptive output feedback controller for flexible-joint robot manipulators, In *2016 IEEE International Conference on Information and Automation (ICIA)*, 2016, vol. 87, pp 1653–1658.
[28] Liu, G. Decomposition-based friction compensation of mechanical systems, *Mechatronics*, 2002, **12**, pp 755–769.
[29] Qiao, B., Qu, H. and Deng, Y. Decentralized robust control of robotic manipulator in joint space based on torque feedbacks, *Arab. J. Sci. Eng.*, 2023, **48**, pp 11277–11284.
[30] Liu, H. and Huang, Y. Robust adaptive output feedback tracking control for flexible-joint robot manipulators based on singularly perturbed decoupling, *Robotica*, 2018, **36**, pp 822–838.
[31] Yu, X.Y. and Chen, L. Modeling and observer-based augmented adaptive control of flexible-joint free-floating space manipulators. *Acta Astronaut.*, 2015, **108**, pp 146–155.
[32] Loria, A. and Ortega, R. On tracking control of rigid and flexible joints robots, Appl. Math. and *Comp. Sci.*, 1995, **5**, pp 329–341.
[33] Liu, Y., Jin, M. and Liu, H. Singular perturbation control for flexible-joint manipulator based on flexibility compensation, Robot, 2008, 30, pp 460–466.
[34] Doetsch, K. Canada's role on space station, *Acta Astronaut.*, 2005, **57**, (2–8), pp 661–675.
[35] Redwire. Redwire awarded contract by European Space Agency to develop robotic arm prototype for Argonaut lunar lander, Redwire Space, May 22, 2024. [Online]. Available: https://redwirespace.com/newsroom/redwire-awarded-contract-by-european-space-agency-to-develop-robotic-arm-prototype-for-argonaut-lunar-lander-to-support-international-lunar-exploration/ [accessed 25 April, 2025].
[36] Dubanchet, V., Romero, J.B., Gregertsen, K.N., et al. EROSS project–European Autonomous Robotic Vehicle for on-orbit servicing. In *International Symposium on Artificial Intelligence, Robotics and Automation in Space, (i-SAIRAS'20)*. Pasadena, California, USA, 2020.
[37] Liu, J., Wang, L. and Wu, Z. Novel study on active reliable PID controller design based on probability density evolution method and interval-oriented sequential optimization strategy, *Comput. Methods Appl. Mech. Eng.*, 2024, **247**, p 117057.
[38] Wang, L., Zhao, Y. and Liu, J. A Kriging-based decoupled non-probability reliability-based design optimization scheme for piezoelectric PID control systems, *Mech. Syst. Sig. Process.*, 2023, **203**, p 110714.

Cite this article: Qiao B., Huang S. and Huang Z. (2025). A singular perturbation-based adaptive control strategy for flexible joint space manipulators with joint friction. *The Aeronautical Journal*, **129**, 3227–3251. https://doi.org/10.1017/aer.2025.10042

https://doi.org/10.1017/aer.2025.10042 Published online by Cambridge University Press